JOURNAL OF CATALYSIS 68, 152–165 (1981)

Criteria for Stable Ni Particle Size under Methanation Reaction Conditions: Nickel Transport and Particle Size Growth via Nickel Carbonyl

W. M. SHEN, J. A. DUMESIC,[1] AND C. G. HILL, JR.

Department of Chemical Engineering, University of Wisconsin, Madison, Wisconsin 53706

Received August 1, 1980; revised October 6, 1980

The loss of methanation activity of alumina-supported nickel catalysts was investigated at pressures up to ca. 600 kPa and temperatures from 400 to 740 K. Deactivation is attributed primarily to growth in nickel particle size. A mechanism involving $Ni(CO)_4$ formation, diffusion, and subsequent decomposition is proposed to explain the observed growth in nickel particle size. A region of "safe" operating conditions for achieving stable catalytic activity for methanation was identified. These safe operating conditions were sensitive to temperature and carbon monoxide partial pressure. A criterion based on the equilibrium partial pressure of $Ni(CO)_4$ is proposed for assessing the safety of a set of operating conditions. Specifically, conditions for which the equilibrium $Ni(CO)_4$ pressure is less than ca. 1×10^{-6} Pa result in stable methanation activity.

INTRODUCTION

Catalytic methanation over nickel has been extensively studied for more than 40 years, from the early work of the British Gas Research Board (*1, 2*) to the more recent work dealing with kinetics, reaction mechanisms and catalyst characterization (*3–15*), and pilot plant studies (*16–18*). Excellent reviews are available in the literature (*19–21*). In commercial applications, considerations of reactor size require that the reaction be carried out at elevated pressures, in the range of 1 to 3 MPa (*22*). Yet, with increasing CO pressure comes the possibility of volatile nickel carbonyl formation. This can lead to a loss of nickel surface area (with concomitant catalyst deactivation) due, for example, to the removal of nickel from the catalyst bed. In this respect, the present paper is a detailed study of catalyst deactivation phenomena attributable to nickel carbonyl formation, from which criteria are offered for maintaining stable nickel surface areas (and hence stable activities) under methanation reaction conditions.

[1] Camille and Henry Dreyfus Foundation Teacher–Scholar. Author to whom correspondence should be addressed.

EXPERIMENTAL METHODS

High-Pressure Reaction System

Kinetic data were measured in the all stainless-steel (type 316) reaction system shown schematically in Fig. 1. The system can be operated at pressures up to 6.8 MPa. The reactor is made of a 1.27-cm-OD × 1.02-cm-i.d. tubing. The use of type 316 stainless steel prevents the formation of $Fe(CO)_5$, and minimizes the formation of $Ni(CO)_4$, from the reaction between CO and the tube wall at high CO pressures and high temperatures (*23*). Composition changes of both reactant mixtures and effluent gases can be monitored continuously using a Gow–Mac high-pressure thermal conductivity cell. The kinetic data were measured after the system had reached steady state, as determined by the steady voltage output from the thermal conductivity cell. The portion of the system downstream from the reactor was wrapped with heating tape to prevent water from condensing. Analyses of both effluent gases and reactant mixtures were carried out us-

0021-9517/81/030152-14$02.00/0

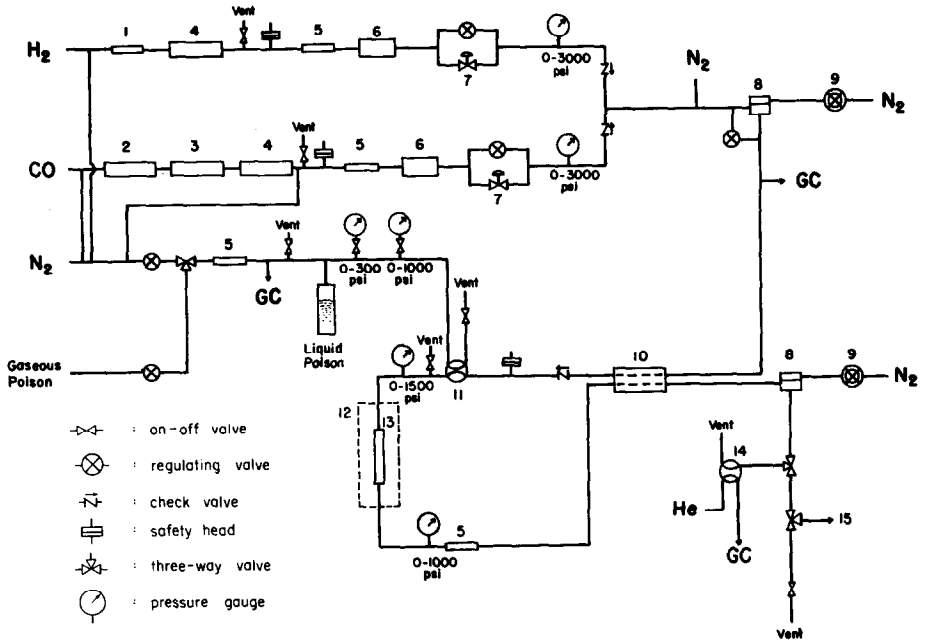

FIG. 1. Schematic diagram of the all stainless-steel system for high-pressure kinetics studies (most on–off valves omitted). 1, Deoxo unit; 2, copper turning trap; 3, 3A molecular sieve trap; 4, 13X molecular sieve trap; 5, filter with 2-μm filter element; 6, Tylan FM-360 flowmeter with readout box RO-14; 7, Chatham precision needle valve; 8, Grove 90W back pressure regulator; 9, Grove 15S small volume regulator; 10, Gow–Mac 10-454-25 WX thermal conductivity cell; with 40-001 power supplier; 11, Valco V-6-HPaX C20 sampling valve; 12, Linberg 54356-V three-zone furnace with 59744-A control console; 13, 316 S.S. tubular reactor; 14, Valco CV-8-HPaX C20 sampling valve; 15, auxiliary exit, which can be connected to wet test meter for flowmeter calibration.

ing a Carle Basic 8700 gas chromatograph operated at 388 K with 1.8 m of 80/100 mesh Spherocarb column.

Hydrogen (National Cylinder Gases) was purified by passage through a Deoxo unit followed by an activated 13X molecular sieve trap at room temperature. Carbon monoxide (Matheson, C.P. grade) was purified by passage through a system composed of a copper turning trap (with 60 cm of preheating section) at 593 K, and activated 3A and 13X molecular sieve traps at room temperature. Such an arrangement was effective in completely removing $Fe(CO)_5$ from the CO stream.

Particle Size Determinations

Hydrogen chemisorption measurements were carried out in an all-glass high-vacuum system described elsewhere (*24*). Prior to chemisorption measurements at room temperature, whether on fresh or used catalysts, the sample was reduced in flowing hydrogen (atmospheric pressure, 50–100 cm^3/min) at 723 K for 1 h, evacuated for 1 h at this temperature, and then cooled under vacuum to room temperature. Desorption isotherms, rather than adsorption isotherms, were measured, because hydrogen chemisorption on Ni involves a fast chemisorption process followed by a slow, activated chemisorption process (*25–27*). A similar procedure has been used for ruthenium (*28*) and nickel–copper catalysts (*29*). The amount of strongly adsorbed hydrogen was estimated by extrapolating the initial portion of the desorption isotherm back to zero pressure. X-Ray diffraction measurements were made on a Picker biplanar diffractometer. Magnetization measure-

ments were carried out using a Cahn RG microbalance and an Alpha model 4800 electromagnet.

Catalyst Preparation and Treatment

Supported nickel catalysts were prepared by incipient wetness impregnation, using 0.6 ml of $Ni(NO_3)_2$ solution per gram of 80/100 mesh γ-Al_2O_3 powder (Davison, SMR-7). After impregnation, the catalysts were dried overnight at 393 K. The "standard" reduction procedure consisted of treating the catalyst in flowing hydrogen (P_{H_2} = 308 kPa) while the sample temperature was (i) slowly increased to 403 K (over a period of 40 min), (ii) held at 403 K for 0.5 h, (iii) held at 533 K for 0.5 h, and (iv) held at 723 K for 2.5 h. The reactor temperature and pressure were then adjusted to the desired values before the H_2/CO reactant mixture was introduced.

Space velocities (at reactor inlet conditions) of 40,000–60,000 $cm^3 \cdot g^{-1} \cdot h^{-1}$ were used to keep CO conversions low so that data analyses could be carried out in terms of a differential reactor model. A procedure similar to that used by Vannice (*12*) was used to maintain a "clean" metal surface. Specifically, after each datum point, CO flow was stopped and H_2 alone was passed over the catalyst surface to effect catalyst regeneration. Typically, the catalyst was exposed to H_2/CO for approximately 0.5 h during the collection of each datum point; this was followed by a 2-h regeneration treatment in H_2. The exit gas was monitored by gas chromatography during this regeneration. It was established that the CH_4 concentration in the H_2 stream dropped to zero within the 2-h regeneration period.

Runs designated by the prefix "A" were carried out using a 10 : 1 mixture of 100/120 mesh γ-Al_2O_3 powder and 80/100 mesh Ni/γ-Al_2O_3 catalyst. The mixture was physically separated using a 100 mesh sieve after the kinetic studies. This separated catalyst was then used for X-ray diffraction and H_2 chemisorption studies. The use of a diluted catalyst allowed the catalyst bed height to be kept nearly constant and CO conversions to be kept low between kinetic runs carried out over greatly different temperature ranges. In the deactivation studies (series A4), the catalyst was not regenerated using hydrogen flushing after each datum point, as had been the procedure in series 2 and 3. This approach made the deactivation studies feasible within a reasonable time span.

Chemical analyses of catalyst samples were carried out by Galbraith Laboratories, Inc.

RESULTS

Experimental conditions are summarized in Table 1. The first digit in the run number designates the batch number of the catalyst preparation. The prefix "A" means that the catalyst studied has been diluted with γ-Al_2O_3 powder. The temperature in parentheses indicates the highest temperature recorded after the reactant mixture was introduced. Temperatures connected by the "→" sign indicate the temperature range studied using step temperature increments of 15 to 25 K from the lower limit to the upper limit. The "time on-stream" refers to the total period of time during which the catalyst was exposed to H_2/CO mixtures under specified conditions. The results of catalyst characterization are summarized in Table 2. The suffix "F" denotes a "fresh" catalyst, which has experienced only standard hydrogen reduction. The values of calculated metal loading are obtained from the concentration and volume of the impregnation solution and the amount of γ-Al_2O_3 powder used for catalyst preparation. Since the height of the catalyst bed was typically 5.1 to 6.4 cm, it was possible to distinguish the upper portion from the lower portion of the catalyst bed. After kinetic studies, the catalyst was removed from the high-pressure reactor. The first half of the catalyst poured out of the reactor was then labeled the upper portion of the catalyst bed, and the second half the

TABLE 1

Experimental Conditions

Run No.	Temp. (K)	Pressure (kPa)		H_2/CO ratio	Time on-stream (min)	Operating regime
		H_2	CO			
2-2	397 → 477	365	123	2.98	132	Unsafe
	723 re-reduction				60	
	474 → 580	378	121	3.12	202	
2-4	428 → 543	381	124	3.07	140	Unsafe
	723 re-reduction				150	
	523 → 598	381	124	3.07	64	
	423	381	124	3.07	22	
2-3	446 → 561	355	117	3.03	236	Unsafe
	723 re-reduction				150	
	457 → 555	352	118	2.99	83	
2-1	527 (728)	461	150	3.07	26	Unsafe
	485 → 529	436	145	3.01	252	
3-1	473	334	79	4.22	100	Unsafe
	723 re-reduction				150	
	473	334	79	4.22	29	
	499	334	79	4.22	49	
A4-8	513	307	85	3.59	930	Unsafe
	562	307	85	3.59	22	
	590	307	85	3.59	17	
A4-6	523	307	85	3.59	124	Unsafe
	547	307	85	3.59	26	
	573	307	85	3.59	17	
A4-12	524	296	81	3.68	128	Unsafe
	549	292	80	3.66	27	
	572	292	80	3.66	23	
	655	294	17.9	16.4	33	Safe
	639 H_2 flushing				72	
	647	294	17.2	17.1	24	
3-2	521 (576)	345	18.6	18.5	44	Safe
	522 (575)	345	19.3	17.9	1487	
A4-11	644	300	17.2	17.4	54	Safe
	741	277	40.7	6.81	50	
	577	300	17.2	17.4	61	
A4-9	653	298	19.3	15.4	930	Safe
	638	298	19.3	15.4	45	
A4-7	651	302	17.9	16.8	49	Safe
	741	285	42.0	6.77	54	

lower portion of the catalyst bed. Such a differentiation between the upper and the lower portions of the catalyst bed was made for runs 2-4 and 3-1.

The rapid loss of activity for methanation at relatively high CO pressure is shown in Fig. 2. These data are characteristic of operation in an "unsafe" regime. Figure 3 shows typical results in the search for "safe" operating conditions. "Safe" oper-

TABLE 2

Catalyst Characterization

Run No.	Metal loading[a] (wt%)		Particle size (nm)			Surface coverage (%)	N_{CH_4}[c] (sec^{-1})
	Calculated	Analytical	XRD		Chemisorption[b]		
			(111)	(200)			
2-2	5.73	0.95	**[d]	—	—	—	—
2-4 upper bed	5.73	3.89	50.3	61.6	—	—	—
2-4 lower bed	5.73	6.51	39.5	35.4	—	—	—
2-3	5.73	5.63	40.1	53.3	—	—	—
2-1	5.73	5.75	33.0	34.9	—	—	—
3-1 upper bed	5.96	5.78	36.9	23.7	—	—	—
3-1 lower bed	5.96	6.34	43.1	23.7	—	—	—
A4-8	5.98	5.44	20.7	12.3	58.1	64	1.5×10^{-3}
A4-6	5.98	5.45	16.4	*	19.8	17	4.1×10^{-3}
A4-12	5.98	—	15.4	*	38.1	60	25.0×10^{-3}
3-2	5.96	—	*[e]	—	—	—	—
A4-11	5.98	—	*	—	7.6	58	31.4×10^{-3}
A4-9	5.98	5.64	*	—	6.5	51	$25.0\text{–}42.6 \times 10^{-3}$
A4-7	5.98	5.82	*	—	6.7	53	—
3F	5.96	—	*	—	4.0	—	—
4F	5.98	6.00	*	—	3.2	—	—

[a] Based on dried-reduced samples.

[b] Assuming spherical particles and 72% reduction (as determined by magnetization measurements). Ni atom area = 6.78 Å^2 (the average of (100), (110), and (111) planes). When possible, the values of metal loading determined by chemical analyses were used for the particle size calculations. For samples 3F, A4-11, and A4-12, the calculated metal loadings were used to calculate Ni particle sizes.

[c] Turnover numbers are extrapolated to T = 548 K, P = 101.3 kPa, and H_2/CO = 3 using Eq. (1).

[d] No Ni diffraction peak can be observed because there is not enough Ni in the sample.

[e] An asterisk denotes that no particle size determination can be made because the peak is too broad. In most cases, the extremely broad Ni diffraction peak cannot be distinguished from background.

ating conditions are defined as those for which the catalyst maintains a stable activity over a period of time long enough for kinetics studies (i.e., several hours exposure to a H_2/CO mixture). Similarly, the "unsafe" operating conditions are those under which the catalyst cannot maintain a stable activity. Thus, a temperature of 688 K is classified as safe, while temperatures of 526 and 588 K are classified as unsafe, when P_{H_2} = 305 kPa and P_{CO} = 18.6 kPa (Fig. 3). The results of the search for safe operating conditions are shown in Fig. 4. For each partial pressure of CO, there is a lower limit in temperature for safe operating conditions. Above this threshold temperature the catalyst does not undergo rapid deactivation in terms of the time frame of our studies. The partial pressure of H_2 plays only a minor role, if any, in the deactivation processes. The deactivation rate remained essentially unchanged when the H_2 pressure was doubled for a run at 602 K and P_{CO} = 33.8 kPa.

After the safe operating regime was mapped, several runs (the A4 series) were designed and carried out to study differences in catalyst structure after use in the safe and unsafe regimes. The most important differences in catalyst structure are those in Ni particle sizes, as determined by X-ray diffraction. The time on-stream is only of minor importance. As indicated in Table 2, the Ni particle sizes for the catalysts after operation in the safe regime (runs 3-2, A4-7, A4-9, and A4-11) are always too

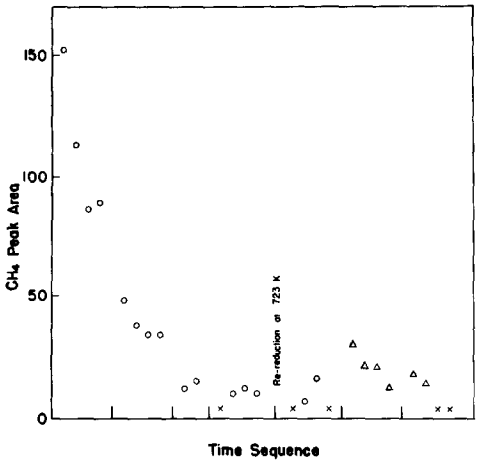

FIG. 2. Rapid loss of catalytic activity for methanation (run 3-1) at 470 (○) and 500 K (△). *X*'s are used for points where CH_4 peaks were so small that they were not integrated by the electronic integrator. Vertical lines on the abscissa denote catalyst regenerations (ca. 2 h) in flowing hydrogen. The catalyst was typically exposed to H_2/CO reactant mixture for 0.5 h between hydrogen regenerations.

small to be determined by X-ray diffraction, regardless of the time on-stream. X-Ray diffraction was also unable to measure the Ni particle sizes in fresh samples (3F and 4F). On the other hand, the Ni particle sizes

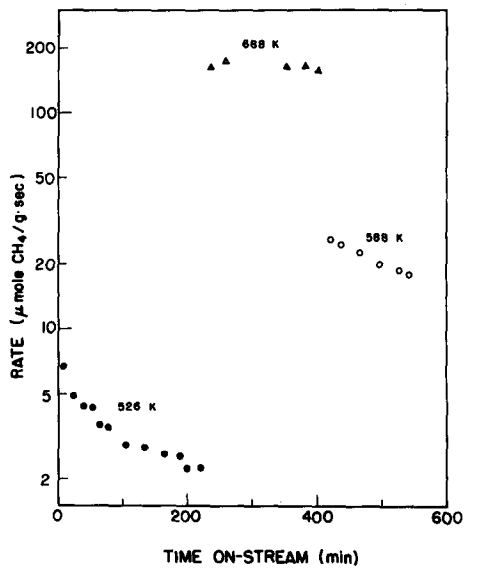

FIG. 3. Safe and unsafe operation conditions for Ni/Al_2O_3 catalyst. P_{H_2} = 305 kPa; P_{CO} = 18.6 kPa.

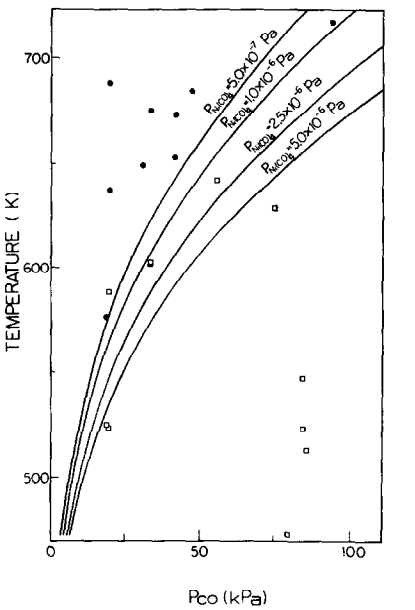

FIG. 4. A map of the region of safe operating conditions for Ni/Al_2O_3 catalysts. (●) Safe operating conditions; (□) unsafe operating conditions. The equilibrium curves for various equilibrium partial pressures of $Ni(CO)_4$ are calculated using thermodynamic data available in the literature.

in the catalysts after operation in the unsafe regime (runs A4-6, A4-8, and A4-12) are always much larger than those in fresh samples. In addition, the Ni particle size in a catalyst after 16 h of operation in the unsafe regime (run A4-8) was not much larger than those obtained after 3 h of treatment in the unsafe regime (runs A4-6 and A4-12). The Ni particle size determinations using H_2 chemisorption always gave larger values than those obtained by X-ray diffraction (Table 2). The calculation of particle size based on H_2 chemisorption has taken into account the fact that not all the Ni present on the alumina support can be reduced to a metallic state. Magnetic measurements indicated that 72% of the Ni loading was reduced to the metallic state during the standard reduction procedure.

The kinetics of the methanation reaction were studied under safe operating conditions in separate experiments using an alumina-diluted catalyst (similar to the A4-

series). Additional studies of the temperature (see Fig. 5) and partial-pressure dependence of the rate (not included in Table 1) indicate that the best fit of the data is of the form

$$r_{CH_4} = A\, e^{(-29{,}000/RT)} P_{H_2}^{0.63} P_{CO}^{0.0}, \qquad (1)$$

where R = 1.987 cal/gmole · K.

DISCUSSION

Nickel Transportation and Particle Size Growth

The calculated values of metal loading agree very well with the results of chemical analyses for runs 2-1, 2-3, and 4F. The small differences between calculated and analytical values in series A-4 are attributable to the physical-separation technique employed. In contrast, the results of the chemical analyses for runs 2-2 and 2-4 are not in agreement with the calculated metal loadings. The Ni metal on the catalyst has been almost completely stripped from the catalyst bed in run 2-2. In run 2-4, the upper portion of the catalyst bed contained far less Ni metal than the calculated value of the metal loading, while the lower portion of the catalyst bed contained far more Ni metal than the calculated value of the metal loading. The average value of the results of the chemical analyses, 5.20%, indicates that there was probably no significant stripping of Ni from the catalyst bed. These phenomena show that Ni can be transported with the gas stream from the upper portion to the lower portion of the catalyst bed, and that, in the extreme case, Ni can even be stripped from the bed.

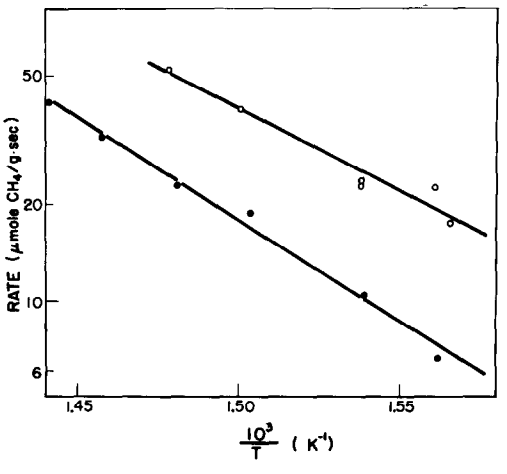

FIG. 5. Arrhenius plots for Ni/Al_2O_3. P_{CO} = 35.8 kPa; P_{H_2} = 257 kPa. (○) Data collected on the first day (E_A = 96 kJ/mole); (●) data collected after catalyst had been on-stream for 21 days (E_A = 121 kJ/mole).

The results from run 3-1 show a more subtle effect of Ni transportation. On one hand, the results of the chemical analyses for run 3-1 indicate that there is only minor Ni transportation. The average value of the metal loading based on chemical analyses, 6.06%, agrees well with the value of the a priori calculation, 5.96%. A small amount of Ni, however, appears to have been transported from the upper to the lower portion of the bed. Yet of major importance is the observation that the Ni particle sizes determined by X-ray diffraction are very large (23–43 nm) compared to the typical size of Ni particles in fresh catalysts (3–4 nm) (Table 2).

Two mechanisms have been proposed for the growth of metal particle sizes in supported catalysts (*30*): The crystal migration model and the interparticle transport model. The crystal migration model (*31, 32*) envisages the growth in particle size as resulting from migration of metal particles over the support surface, followed by collision and coalescence. This model is not believed to be applicable for the conditions of the present study. Specifically, this mechanism requires a high mobility of metal particles on the surface of the support; however, the Tammann temperature of Ni, 964 K, is much higher than the temperatures involved in these runs. Indeed, particle mobility is not generally observed at temperatures below the Tammann temperature (*33*). Furthermore, this model is not consistent with the results of this study, which show that particle size growth becomes less extensive as the temperature is increased (see Tables 2 and 3). For example, the Ni particle size in the

TABLE 3

Thermodynamic Calculations of $Ni(CO)_4$

Run No.	Temp.[a] (K)	P_{CO} (kPa)	$P_{Ni(CO)_4}$[b] (Pa)	Loss of Ni from bed[c]	Transport of Ni down the bed[c]	Ni particle size growth[c,e]	Stable catalytic activity[c]
2-2	397	123	67	*	—	—	—
2-4	423	124	47	*	*	*	—
2-3	446	117	4.5	—	—[d]	*	—
2-1	485	145	0.46	—	—[d]	*	—
3-1	473	79.2	0.10	—	*	*	—
A4-8	513	85.5	8.0×10^{-3}	—	—	*	—
A4-6	523	85.5	4.2×10^{-3}	—	—	*	—
A4-12	524	80.6	3.1×10^{-3}	—	—	*	—
3-2	576	18.6	4.6×10^{-7}	—	—	—	*
A4-11	577	17.2	3.2×10^{-7}	—	—	—	*
A4-9	653	19.3	1.6×10^{-8}	—	—	—	*
A4-7	651	17.9	1.3×10^{-8}	—	—	—	*

[a] The lowest temperature in each run.
[b] Equilibrium partial pressure of nickel carbonyl based on calculated equilibrium constant.
[c] X-Ray diffraction peak observable.
[d] Separation of the upper from the lower portion of the catalyst bed was not attempted.
[e] Asterisk indicates that phenomenon was observed.

catalysts used in runs A4-7, A4-9, and A4-11 (which have experienced temperatures as high as 741 K) is too small to be determined by X-ray diffraction indicating that the temperatures used in this study were not high enough to cause surface migration of metal particles. This conclusion is also supported by reported observations. Richardson and Crump (*34*) showed that the dispersion of a Ni/SiO_2 catalyst was very stable at 673 K in helium. Williams *et al.* (*35*) showed that the nickel surface area of a coprecipitated $Ni–Al_2O_3$ catalyst remained constant during a 1000-h treatment at 673 K in a steam and hydrogen mixture. It also remained constant during treatment at 1073 K in hydrogen. Temperatures in both studies were higher than the temperatures employed in runs 2-2, 2-4, and 3-1.

The second model for particle size growth, the interparticle transport model (*36, 37*) involves escape of atomic or molecular metal species from crystallites, migration of these species along the surface (or vapor-phase transport), and their recapture by crystallites via collision or readsorption. A mechanism similar to the interparticle transport model is postulated to explain the phenomena observed in the present studies. Upon exposure to an appropriate H_2/CO reactant mixture, the Ni metal particle reacts with adsorbed CO or with CO molecules in the gas phase to form $Ni(CO)_4$ species. The formation of $Ni(CO)_4$ from Ni on SiO_2 maintained in a CO atmosphere has been reported by Vannice and Garten (*38*). The formation of $Ni(CO)_4$ under room temperature CO chemisorption conditions indicates the ease with which it is formed (*39*). Van Meerten *et al.* (*40*) have in fact raised the possibility of having $Ni(CO)_4$ as an intermediate for the transport of Ni from small to large Ni particles in a Ni on SiO_2 catalyst. Product $Ni(CO)_4$ molecules can leave the metal particle and diffuse through the gas phase and/or over the catalyst support. Depending on the operating conditions, these species then decompose to metallic Ni on either a nearby Ni particle or a Ni particle on a catalyst granule downstream from the original. Indeed, $Ni(CO)_4$ partially decomposes at temperatures as low as 298–303 K (*41*). Derouane *et al.* (*42*) studied the preparation of

Ni catalysts by decomposing $Ni(CO)_4$ on Al_2O_3 fibers at 473 K. The industrial production of high-purity Ni pellets is carried out by decomposing $Ni(CO)_4$ at 443–523 K (*43*). Temperatures employed in most of our runs are higher than these decomposition temperatures. Finally, under certain conditions, the $Ni(CO)_4$ molecules may even be flushed out of the reactor, causing the stripping of Ni metal from the catalyst bed as will be discussed later.

As pointed out earlier, one of the prominent differences between catalysts after operation in the safe regime and catalysts after operation in the unsafe regime is the Ni particle size determined by X-ray diffraction. After 16 h of treatment at 653 K in the safe regime (run A4-9) a catalyst still has a Ni particle size comparable to that of a fresh sample. However, after 3 h of treatment at lower temperatures in the unsafe regime (run A4-6) a catalyst shows a five-fold increase in Ni particle size relative to those of fresh samples. As can be seen in Tables 1 and 2, the correlating factors are (i) the CO partial pressure, which was higher in the unsafe treatments than in the safe treatments, and (ii) the temperature, which was lower in the unsafe treatments than in the safe treatments. Thermodynamically the higher CO pressure and the lower temperature used in the unsafe treatment favor the formation of $Ni(CO)_4$. These data are consistent with the argument that the deactivation proceeds via the interparticle transport model rather than via the crystallite migration model.

Kinetic and Thermodynamic Aspects of $Ni(CO)_4$ Formation

Thermodynamic data for the reaction

$$Ni + 4CO_{(g)} \rightleftarrows Ni(CO)_{4\,(g)}$$

are available in the literature (*44–48*). The data summarized by Goldberger and Othmer (*47*) were used for calculating equilibrium partial pressures of $Ni(CO)_4$. The calculated values are tabulated in Table 3.

Goldberger and Othmer (*47*) found that the rate of $Ni(CO)_4$ formation reaches a maximum at 348 K at all CO pressures studied, while Kipnis *et al.* (*49*) and Kipnis and Mikhailova (*50*) have determined the kinetic rate expression for this reaction. Accordingly, for all runs in the present study, the rate of $Ni(CO)_4$ formation would be approximately 10^{-6} mole/cm^2 · h in the *absence* of gaseous $Ni(CO)_4$. This corresponds to about 10^2 monolayers of Ni removed from each Ni particle per hour. (These kinetic data are only semiquantitative due to the fact that a much larger Ni particle size, 38 μm, was used in the studies of Kipnis *et al.* (*49*) and of Kipnis and Mikhailova (*50*).) Yet, small Ni particles (consisting of several tens of monolayers) are in fact stable for long times in runs 3-2, A4-11, A4-9, and A4-7. Thus, the kinetics of $Ni(CO)_4$ decomposition must also be considered in interpreting the phenomena of the present study. In short, it has been found (*51–54*) that the rate increases with increasing temperature up to approximately 400 K, while above this temperature the rate-determining step in the thermal decomposition is the gas-phase diffusion of $Ni(CO)_4$ to the surface of metallic nickel (*51, 53*). In other words, the intrinsic rate of $Ni(CO)_4$ decomposition on metallic Ni at temperatures higher than ca. 400 K is fast compared to the rate of gas-phase diffusion of $Ni(CO)_4$ to the Ni surface. In the present case, the fast rates of $Ni(CO)_4$ formation and decomposition suggest that thermodynamic equilibrium with respect to formation of $Ni(CO)_4$ from nickel and carbon monoxide is achieved at the surface of the Ni particles during methanation.

The equilibrium partial pressures of $Ni(CO)_4$ vary from 67 Pa for the run in which Ni was stripped from the catalyst bed to 1.3×10^{-8} Pa for a run in the safe regime. Under those conditions for which the thermodynamics of $Ni(CO)_4$ formation are unfavorable (small $Ni(CO)_4$ partial pressure), the flux of $Ni(CO)_4$ away from each Ni particle is expected to be small. The Ni

particle size distribution is then stable, because the various particles do not exchange nickel via $Ni(CO)_4$ transport. When the reaction conditions are changed such that the $Ni(CO)_4$ partial pressure at the Ni surface is increased, the flux of $Ni(CO)_4$ away from the Ni particles is expected to increase. However, as long as the decomposition of $Ni(CO)_4$ is fast compared to the rate of diffusion, the $Ni(CO)_4$ will subsequently decompose near the site at which it was formed. This provides a mechanism for exchange of Ni between neighboring Ni particles. There would not be any growth in particle size if $Ni(CO)_4$ decomposed at the same rate on Ni particles having different sizes. However, the rate at which a particle gains metal atoms by the processes described in the interparticle transport model is proportional to the effective diameter of the particle (*36*). Kipnis and Mikhailova (*46*) have reported that nickel carbonyl is easier to form from smaller Ni particles. Hence one expects larger particles to grow at the expense of smaller ones, and this is the mechanism by which the Ni particle size increases. This expectation is confirmed by observations of Evans and Simpson (*55*) on an industrial process producing Ni pellets via decomposition of $Ni(CO)_4$. Finally, as the temperature is decreased, the intrinsic rate of $Ni(CO)_4$ decomposition decreases faster than the rate of $Ni(CO)_4$ diffusion. This allows the $Ni(CO)_4$ to diffuse and decompose further from the site at which it was originally formed. At sufficiently low temperatures, the $Ni(CO)_4$ would be able to diffuse out of the catalyst granule in which it was formed, and then be decomposed in another granule further downstream in the catalyst bed. In the limiting case of slow intrinsic rates of $Ni(CO)_4$ decomposition, the $Ni(CO)_4$ would be swept from the catalyst bed by the gas flowing through the reactor.

Inspection of Table 3 shows that the experimental observations are in accord with the above arguments. The various experimental runs are listed in the order of decreasing equilibrium $Ni(CO)_4$ partial pressures for the temperatures and CO partial pressures used in the methanation studies. The presence of an asterisk as an entry in the table indicates that one or more of the following phenomena were observed in the run in question: (i) loss of Ni from the catalyst bed, (ii) transport of Ni down the catalyst bed, (iii) growth of Ni particle size, and (iv) stable nickel particle size and catalytic activity.

It can be seen that those runs with the highest $Ni(CO)_4$ partial pressures combined with the slowest intrinsic $Ni(CO)_4$ decomposition rates showed the most dramatic effects of Ni transportation. (The intrinsic rate of $Ni(CO)_4$ decomposition, which increases with increasing temperatures, is used for comparison among various runs, since the effect of $Ni(CO)_4$ diffusion is considered separately.) For example, the conditions of run 2-2 corresponded to the highest equilibrium $Ni(CO)_4$ partial pressure with the slowest $Ni(CO)_4$ decomposition rate, and significant loss of Ni from the catalyst bed was observed in this run. Run 2-4 had a smaller $Ni(CO)_4$ equilibrium partial pressure with a higher $Ni(CO)_4$ decomposition rate; less removal of Ni from the bed was observed. On the other hand, significant transport of Ni down the catalyst bed was observed during this run. The equilibrium $Ni(CO)_4$ partial pressure of run 3-1 was still lower while the $Ni(CO)_4$ decomposition rate was higher; less extensive Ni transport down the catalyst bed was observed, compared to that of run 2-4. Furthermore, no loss of Ni from the catalyst bed was observed for run 3-1. The conditions of runs A4-8, A4-6, and A4-12 gave equilibrium $Ni(CO)_4$ partial pressures lower than those of run 3-1. Accordingly, no transport of Ni out of the catalyst bed or down the catalyst bed was observed. However, the Ni particles were observed to increase in size under these reaction conditions. That is, the equilibrium $Ni(CO)_4$ partial pressure was still high enough to allow Ni particles within a given catalyst granule

to exchange matter via $Ni(CO)_4$ transport. Finally, the lowest equilibrium $Ni(CO)_4$ partial pressures were those of runs 3-2, A4-11, A4-9, and A4-7. Indeed, the size of Ni particles did not increase and the catalysts maintained stable activity during each of these runs. The temperatures and CO partial pressures of these runs correspond to safe operating conditions.

Figure 4 shows calculated equilibrium partial pressure curves for $Ni(CO)_4$ as a function of temperature and CO partial pressure. The equilibrium curve for $P_{Ni(CO)_4} = 1.0 \times 10^{-6}$ Pa outlines the border between the safe operating regime and the unsafe regime. This is to be expected, because, as mentioned earlier, thermodynamics plays an important role in determining the conditions for safe operation. Thus, the equilibrium partial pressure of $Ni(CO)_4$ can be used as an empirical criterion for determining the "safety" of a given set of operating conditions.

Similar deactivation behavior has been observed for a commercial 30% Ni/α-Al_2O_3 catalyst (*15*) and a 5% Ni/Al_2O_3 monolithic catalyst (*56*). The corresponding equilibrium $Ni(CO)_4$ partial pressures are 7.18×10^{-2} Pa and 2.7×10^{-6} to 1.3×10^{-5} Pa, respectively. These values are larger than the suggested safe value of 1.0×10^{-6} Pa. Van Meerten *et al.* (*40*) have recently shown by magnetization measurements that the Ni particle size of a 4.88% Ni/SiO_2 catalyst grows gradually during methanation. The equilibrium $Ni(CO)_4$ partial pressure corresponding to their operating conditions is 4.0×10^{-6} Pa. These facts suggest that the present criterion for judging the "safety" of operating conditions can be applied to other systems with higher metal loadings and/or different geometry. The previously stated conclusion concerning the insensitivity of this deactivation process to the hydrogen partial pressure is also supported by these studies. Vannice and Garten (*15*) used a partial pressure of H_2 which is twice that employed in this study. Bartholomew (*56*) found no difference in deactivation behavior between runs with $H_2/CO = 2$ and those with $H_2/CO = 3$.

Blockage of Surface Sites

For Al_2O_3-supported catalysts the larger Ni particle sizes determined by hydrogen chemisorption relative to those determined by X-ray diffraction have been previously attributed to metal-support interactions, e.g., formation of a surface spinel (*14*). Hence, magnetization measurements were used to study the reducibility of a typical Ni/Al_2O_3 catalyst. After the standard reduction procedure a catalyst showed 72% reducibility (run 4F). This value was used to correct the metal loadings used for calculating the particle size based on H_2 chemisorption. For a freshly reduced sample (4F) the particle size determined by H_2 chemisorption is 3.2 nm, a value which agrees very well with those determined by magnetization measurements. The Langevin low-field estimate at 300 K gives 3.4 nm, while the Langevin high-field estimate at 77 K gives 2.8 nm. However, after exposure to H_2/CO reaction mixtures, the reducibility-corrected Ni particle sizes determined by hydrogen chemisorption are consistently larger than those determined by X-ray diffraction. The difference is too large to be attributed to experimental uncertainty and it cannot be explained by the presence of a particle size distribution. The catalyst surface must be blocked, probably by carbon deposition. In estimating the percentage coverages of the surface (see Table 2), it is assumed that the actual Ni particle size after operation in the safe regime is the same as that for run 4F, and that the Ni particles are spherical. The first assumption is suggested by the fact that these catalysts are indistinguishable by X-ray diffraction measurements. The X-ray diffraction data, however, were suggestive of nonspherical particles in several cases, e.g., runs 3-1 and A4-8. While the assumption of a spherical particle shape may invalidate the quantitative aspects of the surface coverage calcu-

lations, the qualitative trends in the values for catalysts exposed to different operating conditions can still be observed. (It is noted that the calculated surface coverages are sensitive to the particle shape assumed.) In short, the extent of surface blockage (by carbon) is approximately the same, after catalyst operation in either safe or unsafe regimes. This adds further support to the belief that the primary difference between the safe and unsafe operating conditions is the extent of Ni particle growth, and not differences in the extent of surface coverage by carbon.

Methanation Kinetics

The Arrhenius plots shown in Fig. 5 indicate that the catalyst activity decreased by only 50% after 21 days on-stream. The activation energy increased by 25 kJ/mole during this mild deactivation process. The activation energy for methane formation is presently reported to be 121 kJ/mole, instead of 96 kJ/mole, because most of the kinetic data were collected after long times on-stream. This value is within the range of reported values for Al_2O_3-supported Ni catalysts (*14*). The dependence of the rate on reactant partial pressures is somewhat different from that reported for kinetic studies at lower temperatures (*14*). However, for methanation, as the results of Bartholomew (*56*) indicate, the partial-pressure dependence is a function of the temperature studied. For purposes of comparison the turnover numbers for methane formation are extrapolated and reported at the conditions used by Vannice (*14*). For catalysts employed in the safe region (runs A4-9 and A4-11), the values agree well with reported values. However, for catalysts employed in the unsafe region (runs A4-6 and A4-8) the values are an order of magnitude lower than reported values, although they agree with each other. In run A4-12, the catalyst had first experienced the same treatments as employed in run A4-6 (see Table 1). The catalyst was then brought into the safe region. The turnover number for the datum point collected in the safe region was indistinguishable from those for catalysts that never had been exposed to operation in the unsafe regime. This fact may indicate that the mechanism of methanation in the unsafe region is different from that in the safe region. Consequently, the use of the rate expression determined from operation in the safe region for data extrapolation of runs in the unsafe regime can give erroneous results.

CONCLUSIONS

The conditions of the present study can be divided into two different operating regimes. In the "safe" regime, the nickel particles are stable against increases in size and the catalytic activity for methanation is constant with time. In the "unsafe" regime, the catalyst deactivates with time due to the increase in Ni particle size. Approximately 50% of the Ni surface is covered by inactive carbon, but this is the same during operation of the catalyst in both safe and unsafe regimes. Particle size growth in Ni/Al_2O_3 methanation catalysts during operation in the unsafe region results from the formation of $Ni(CO)_4$, diffusion of this species through the gas phase and/or over the catalyst surface, and subsequent decomposition of $Ni(CO)_4$. Thermodynamic considerations can be used to predict whether a given set of reaction conditions corresponds to the safe or unsafe regime of operation. Specifically, conditions for which the equilibrium partial pressure of $Ni(CO)_4$ is less than ca. 10^{-6} Pa will give stable methanation activity for catalysts consisting of nickel on alumina. Conversely, reaction conditions giving much higher equilibrium partial pressures of $Ni(CO)_4$ will lead to transport of nickel through the catalyst bed and ultimately to the removal of nickel from the catalytic reactor. In addition, the mechanism of

methanation in the unsafe regime may be different from that in the safe regime.

ACKNOWLEDGMENTS

We would like to thank Mr. J. E. Kubsh for carrying out the magnetization measurements, and Dr. R. J. Madon for encouraging discussions during the early stages of this study. Financial support from the National Science Foundation (Specialized Equipment Grant ENG 77-16850) and Department of Energy (ET-78-G-01-3380) are also gratefully acknowledged.

REFERENCES

1. Report of director, year ending March 31, 1939, British Fuel Research Board, p. 118.
2. Dent, F. J., and Hebden, D., British Gas Research Board, communication GRB 51, 1950.
3. Randhava, S. S., Camara, E. H., and Rehmat, A., *Ind. Eng. Chem. Prod. Res. Develop.* **8**, 347 (1969).
4. Randhava, S. S., Rehmat, A., and Camara, E. H., *Ind. Eng. Chem. Process Des. Develop.* **8**, 482 (1969).
5. Van Herwijnen, T., Van Doesburg, H., and De-Jong, W. A., *J. Catal.* **28**, 391 (1973).
6. Vlasenko, V. M., Yuzefovich, G. E., and Rusov, M. T., *Kinet. Katal.* **6**, 688 (1965).
7. Schoubye, P., *J. Catal.* **14**, 238 (1969).
8. Schoubye, P., *J. Catal.* **18**, 118 (1970).
9. Kreindel, A. I., Sobolevskii, V. S., Golosman, E. Z., and Yakerson, V. I., *Kinet. Katal.* **15**, 408 (1974).
10. Dalla Betta, R. A., Piken, A. G., and Shelef, M., *J. Catal.* **35**, 54 (1974).
11. Dalla Betta, R. A., Piken, A. G., and Shelef, M., *J. Catal.* **40**, 173 (1975).
12. Vannice, M. A., *J. Catal.* **37**, 449 (1975).
13. Vannice, M. A., *J. Catal.* **37**, 462 (1975).
14. Vannice, M. A., *J. Catal.* **44**, 152 (1976).
15. Vannice, M. A., and Garten, R. L., *Ind. Eng. Chem. Prod. Res. Develop.* **18**, 186 (1979).
16. Haynes, W. P., Forney, A. J., Elliott, J. J., and Pennline, H. W., *Adv. Chem. Ser.* **146**, 87 (1975).
17. Schehl, R. R., Pennline, H. W., Strakey, J. P., and Haynes, W. P., *Amer. Chem. Soc. Div. Fuel Chem. Prepr.* **21**(4), 2 (1976).
18. Haynes, W. P., Schehl, R. R., Weber, J. K., and Forney, A. J., *Ind. Eng. Chem. Process Des. Develop.* **16**, 113 (1977).
19. Mills, G. A., and Steffgen, F. W., *Catal. Rev.* **8**, 159 (1973).
20. Vlasenko, V. M., and Yuzefovich, G. E., *Russ. Chem. Rev.* **38**, 728 (1969).
21. Vannice, M. A., *Catal. Rev.* **14**, 153 (1976).
22. Satterfield, C. N., "Heterogeneous Catalysis in Practice." McGraw-Hill, New York, 1980.
23. Inouye, H., and DeVan, J. H., *J. Mater. Energy Syst.* **1**, 52 (1979).
24. Lund, C. R. F., Schorfheide, J. J., and Dumesic, J. A., *J. Catal.* **57**, 105 (1979).
25. Schuit, G. C. A., and DeBoer, N. H., *Rec. Trav. Chim. Pays-Bas* **70**, 1067 (1951).
26. Rostrup-Nielsen, J. R., "Steam Reforming Catalyst." Teknisk Forlag A/S, Copenhagen, 1975.
27. Bartholomew, C. H., and Farrauto, R. J., *J. Catal.* **45**, 41 (1976).
28. Dalla Betta, R. A., *J. Catal.* **34**, 57 (1974).
29. Dalmon, J. A., *J. Catal.* **60**, 325 (1979).
30. Wynblatt, P., and Gjostein, N. A., *Progr. Solid State Chem.* **9**, 21 (1975).
31. Ruckenstein, E., and Pulvermacher, B., *AIChE* **19**, 356 (1973).
32. Ruckenstein, E., and Pulvermacher, B., *J. Catal.* **29**, 224 (1973).
33. Baker, R. T. K., *Catal. Rev. Sci. Eng.* **19**, 161 (1979).
34. Richardson, J. T., and Crump, J. G., *J. Catal.* **57**, 417 (1979).
35. Williams, A., Butler, G. A., and Hammonds, J., *J. Catal.* **24**, 352 (1972).
36. Flynn, P. C., and Wanke, S. E., *J. Catal.* **34**, 390 (1974).
37. Flynn, P. C., and Wanke, S. E., *J. Catal.* **34**, 400 (1974).
38. Vannice, M. A., and Garten, R. L., *J. Catal.* **56**, 236 (1979).
39. Bartholomew, C. H., "Quarterly Technical Progress Report." Department of Energy, Contract EF-77-S-01-2729, July, 1979.
40. Van Meerten, R. Z. C., Habets, H. M. J., Beaumont, A. H. G. M., and Coenen, J. W. E., *in* "Proceedings, 7th International Congress on Catalysis, Tokyo, Japan, 1980," preprint.
41. Syrkin, V. G., Vasilenok, E. M., and Tolmasskii, I. S., *Porosh. Met.* **3**, 6 (1970).
42. Derouane, E. G., Nagy, J. B., and Védrine, J. C., *J. Catal.* **46**, 434 (1977).
43. Forman, H. R., U.S. Patent 3,826,225, July 30, 1974.
44. Syrkin, V. G., *Russ. J. Phys. Chem.* **48**, 1718 (1974).
45. Ross, L. W., Haynie, F. H., and Hochman, R. F., *J. Chem. Eng. Data* **9**, 339 (1964).
46. Kipnis, A. Ya., and Mikhailova, N. F., *Zh. Prikl. Khim.* **45**, 1450 (1972).
47. Goldberger, W. M., and Othmer, D. F., *Ind. Eng. Chem. Process Des. Develop.* **2**, 202 (1963).
48. Spice, J. E., Staveley, L. A. K., and Harrow, G. A., *J. Chem. Soc.*, 100 (1955).
49. Kipnis, A. Ya., Mikhailova, N. F., and Ravdel, A. A., *Kinet. Katal.* **8**, 803 (1967).

50. Kipnis, A. Ya., and Mikhailova, N. F., *Kinet. Katal.* **12,** 1397 (1971).
51. Carlton, H. E., and Oxley, J. H., *AIChE J.* **13,** 86 (1967).
52. Kalitovich, I. M., Kipnis, A. Ya., Mikhailova, N. F., and Taganov, D. N., *Zh. Prikl. Khim.* **47,** 43 (1974).
53. Tsylov, B. A., *Porosh. Met.* **5,** 21 (1971).
54. Goosen, A. J., and Van der Berg, J. A., *J. S. Afr. Chem. Inst.* **25,** 370 (1972).
55. Evans, D., and Simpson, A. B., U.S. Patent 3,844,251, October 29, 1974.
56. Bartholomew, C. H., "Quarterly Technical Progress Report." Department of Energy, Contract EF-77-S-01-2729, January, 1980.